Asymmetric azide-alkyne Huisgen cycloaddition on chiral metal surfaces

Samuel Stolz[1,2], Michael Bauer[3], Carlo A. Pignedoli[1], Nils Krane[1], Max Bommert[1], Elia Turco[1], Nicolo Bassi[1], Amogh Kinikar[1], Néstor Merino-Dìez[1], Roland Hany[3], Harald Brune[2], Oliver Gröning[1], and Roland Widmer[1,*]

[1]Empa, Swiss Federal Laboratories for Materials Science and Technology, nanotech@surfaces Laboratory, 8600 Dübendorf, Switzerland

[2]Institute of Physics, École Polytechnique Fédérale de Lausanne, CH-1015 Lausanne, Switzerland

[3]Empa, Swiss Federal Laboratories for Materials Science and Technology, Laboratory for Functional Polymers, 8600 Dübendorf, Switzerland

Achieving fundamental understanding of enantioselective heterogeneous synthesis is marred by the permanent presence of multitudinous arrangements of catalytically active sites in real catalysts. In this study, we address this issue by using structurally comparatively simple, well-defined, and chiral intermetallic PdGa{111} surfaces as catalytic substrates. We demonstrate the impact of chirality transfer and ensemble effect for the thermally activated azide-alkyne Huisgen cycloaddition between 3-(4-azidophenyl)propionic acid and 9-ethynylphenanthrene on these threefold symmetric intermetallic surfaces under ultrahigh vacuum conditions. Specifically, we encounter a dominating ensemble effect for this reaction as on the Pd_3-terminated PdGa{111} surfaces no stable heterocoupled structures are created, while on the Pd_1-terminated PdGa{111} surfaces, the cycloaddition proceeds regioselectively. Moreover, we observe chirality transfer from the substrate to the reaction products, as they are formed enantioselectively on the Pd_1-terminated PdGa{111} surfaces. Our results evidence a determinant ensemble effect and the immense potential of PdGa as asymmetric heterogeneous catalyst.

In recent years, on-surface synthesis under ultrahigh vacuum (UHV) conditions has emerged as a very successful method to produce extended, covalently bonded macro-molecules, which are inaccessible to wet-chemical synthesis due to insolubility or high reactivity.[1] On-surface synthesis is based on the controlled reaction of dedicated precursor molecules on well-defined single crystal surfaces mostly by thermal activation. Although in recent years, the catalogue of on-surface reactions and synthesized structures broadened extensively, the focus rarely lay on enantioselective synthesis, which is of immense importance for instance in pharmaceutical, agricultural, or food industry.[2,3] This lack of enantioselective on-surface synthesis originates largely from the scarcity of intrinsically chiral, catalytically active, and well-characterized single-crystal surfaces needed for this task. One option to circumvent this deficiency is to render achiral surfaces chiral via the adsorption of enantiopure molecules.[4–10] This approach has proven very successful under ambient conditions for instance in the asymmetric hydrogenation of activated ketones and asymmetric hydrogenation of prochiral olefins.[11]

Intrinsically chiral metal surfaces promise an increased thermal stability, a reduction of complexity arising from the multitude of molecule-molecule arrangements and interactions, and would not require enantiopure molecular modifiers, but are accompanied by a reduced adjustability towards specific reactions. In this context, high Miller-index surfaces of achiral crystals,[12,13] which exhibit a low density of chiral centers only at the kink sites of atomic steps separating adjacent terraces of low-index surfaces, have been established for enantioselective decomposition reactions under UHV conditions. [14,15]

Low Miller-index surfaces of intrinsically chiral bulk crystals possess a high density of well-defined and thermally stable chiral centers. Even though chiral metallic crystals gain increasing attention in the context of topological electronic properties,[16–23] in-depth characterization of their surface structure is very limited. Currently, the only intrinsically chiral and catalytically active single-crystal whose low-index surfaces are well-characterized is intermetallic PdGa. PdGa belongs to the non-centrosymmetric space-group $P2_13$,[24] and thus exists in two enantiomorphs, denoted as PdGa:A and PdGa:B.[25] Here, we focus on the two structurally dissimilar, bulk-truncated, three-fold symmetric PdGa:A($\bar{1}\bar{1}\bar{1}$) and PdGa:A(111) surfaces, of which the former is terminated by isolated Pd trimers, further referred to as A:Pd$_3$ (Fig. 1a), while the top layer of the latter consists of single, isolated Pd atoms, and is denoted A:Pd$_1$ (Fig. 1b).[26] Owing to their differing surface terminations, in combination with their equal lattice parameters, identical symmetry, and similar electronic properties, the PdGa{111} surfaces are ideally suited to disentangle ensemble and ligand effects, i.e., the influence of the local geometric and electronic properties, respectively, in asymmetric heterogeneous catalysis.[27–30]

Chirality transfer from the PdGa{111} surfaces onto molecular processes has been demonstrated with acetylene (C_2H_2; achiral) and 9-ethynylphenanthrene (9-EP; prochiral, thus appearing in two distinguishable surface enantiomers R and S when confined to a planar configuration).[31–33] Specifically, C_2H_2 has been reported to exhibit directed rotation on the Pd$_3$-terminated PdGa{111} surfaces.[31] On the other hand, for 9-EP, enantiopure trimerization from an initial racemic mixture of monomers on the Pd$_3$- and enantioselective adsorption of individual monomers on the Pd$_1$-terminated PdGa{111} surfaces have been shown.[32,33]

Therefore, 9-EP promotes itself as prototypical alkyne precursor for investigating enantioselective synthesis on the PdGa{111} surfaces. Moreover, on-surface azide-alkyne Huisgen cycloaddition (Fig. 1c) without emphasis on enantioselectivity, has been successfully demonstrated on Au(111),[34] and, using 9-EP as precursor, on Cu(111) under UHV conditions by Bebensee *et al.*.[35] This catalytically activated reaction, which belongs to the class of Click Chemistry, selectively yields 1,4-triazole regioisomers and omits the formation of 1,5-triazoles. According to the d-band model introduced by Nørskov *et al.*,[28,36] PdGa is expected to possess similar catalytic activity for the azide-alkyne Huisgen cycloaddition as copper. To

73 perform the reaction, we chose commercially available prochiral 3-(4-azidophenyl)propionic acid (APA) as
74 azide reactant (Fig. 1d).

75 Using scanning tunneling microscopy (STM), complemented with x-ray photoelectron spectroscopy (XPS),
76 and density functional theory (DFT) calculations, we demonstrate a significant ensemble effect on the
77 PdGa{111} surface reactivity, manifested in the occurrence of the regio- and, most importantly,
78 enantioselective cycloaddition between APA and 9-EP on the Pd_1-terminated PdGa{111} surfaces, but its
79 suppression on Pd_3-terminated PdGa{111}.

80 A series of STM images of the individual deposition of 9-EP and APA molecules and the co-deposition of
81 both molecules on A:Pd_3 at room temperature (RT) and after subsequent annealing to 425 K and 515 K is
82 shown in Figure 2. As previously reported,[32] 9-EP deposited at RT results in a homogeneous racemate of
83 well isolated monomers (Fig. 2a) and formation of 9-EP trimers with increasing enantiomeric excess (ee)
84 up to 97% ± 2% towards RRR enantiomorphs for increasing temperatures (Fig. 2b,c). On the other hand,
85 APA molecules deposited on A:Pd_3 at RT create large, disordered agglomerates (Fig. 2d). Additionally,
86 depressions, which are absent on the pristine surface, are observed on the substrate, as indicated by the
87 white arrow. We attribute these depressions to fragments of the decomposed carboxylic acid group of the
88 APA molecule as they are also observed upon deposition of ex-situ synthesized 1,4-triazoles (Fig. S1) and
89 XPS investigations show a strong C 1s component arising from the carboxylic acid group (Fig. S2). On the
90 other hand, the ratio between the C 1s and N 1s XPS intensity is around three times larger than the one
91 expected for pristine APA (Table S4). Hence also most azide groups decompose, and desorb from the
92 surface. Subsequent annealing of the sample up to 515 K leads to a reduction of the depressions, as they
93 desorb, while agglomeration proceeds without ever forming discernible regular structures, i.e.,
94 reoccurring structures of similar topographic signature in STM images (Fig. 2d-f).

95 When APA is co-deposited with 9-EP on A:Pd_3, no intermolecular reactions are observed at RT. While APA
96 again agglomerates, 9-EP seems to mostly bond to the previously mentioned molecular fragments
97 detached from APA molecules (depressions), as pointed out by the green arrow in Fig. 2g. Upon annealing
98 to 425 K (Fig. 2h), 9-EP appears in its pristine adsorption configuration, which means it is detached from
99 the molecular fragments, and, importantly, new prochiral 9-EP/APA heterostructures that consist of two
100 9-EP and one APA molecule are formed (Fig. 2j-k). The adsorption configuration of 9-EP molecules
101 incorporated in these trimer heterostructures with respect to the PdGa substrate is identical with that
102 reported in Ref.[32] for R enantiomers incorporated into pure 9-EP trimers. The heterostructure trimers
103 exclusively appear in the enantiomeric form shown in Fig. 2j-k on the A:Pd_3 termination. The incorporated
104 APA is not covalently bound in these heterostructure trimers, as, upon further annealing to 515 K, these
105 structures deplete and homostructural 9-EP trimers become the only regular motive (highlighted by a
106 green circular arrow in Fig. 2i). Therefore, even though PdGa is copper-like with regard to the catalytic
107 reactivity according to the d-band model,[36] the azide-alkyne Huisgen cycloaddition cannot be triggered
108 with any significant yield on the A:Pd_3 surface.

109 On the A:Pd_1 surface, 9-EP deposited at RT adsorbs with an *ee* of 98 % in favor of the R enantiomer (cf. Fig.
110 3a), and dimerizes without *ee* above 400 K, as reported by Prinz *et al.*.[37] The adsorption behavior of APA
111 on the Pd_1-terminated PdGa{111} surfaces is in stark contrast to that on A:Pd_3, as the APA molecules barely
112 agglomerate even at temperatures up to 415 K (Fig. 3b, S5). The most frequently observed APA structures
113 are shown in the STM images in Fig. 3c-f. The sickle-like molecular structures in Fig. 3c,e strongly resemble
114 the terminal phenylpropionic acid group of the ex-situ synthesized 1,4-triazoles adsorbed on
115 PdGa:A(111)Pd_1 in Fig. S10. These two structures are attributed to pristine APA molecules, whereas their
116 azide group only exhibits a very weak STM signal like on the less corrugated Ag(111) in Ref. [38]. The coverage
117 of the molecular structures in Fig. 3c,e relative to all APA derivatives on the Pd_1-terminated PdGa{111}

118   surfaces amounts to around 30-35%, upon deposition and after annealing to 415 K (Fig. S5), which is in
119   good agreement with the maximum amount of pristine APA molecules estimated from XPS investigations
120   (Table S5). The molecular structures in Fig. 3d,f are APA molecules with decomposed azide group. On Pd_1-
121   terminated PdGa{111} surfaces, part of the APA propionic acid groups are deprotonated (Fig. S2, Table
122   S2), but no signs of their detachment from APA molecules could be identified, neither with XPS nor STM.

123   After having clarified that around 30% of the APA monomers remain structurally intact up to 415 K on the
124   Pd_1-terminated PdGa{111} surfaces, APA was co-deposited with 9-EP at RT (Fig. 4). As shown in Fig. 4a,
125   both 9-EP and APA mainly appear as non-interacting monomers. The pronounced depressions on this
126   surface represent Pd vacancies in the Pd_1-termination[26] and the apparent trimer is composed of individual
127   9-EP molecules adsorbed on such a vacancy.[37] 9-EP molecules appear with a relative abundance between
128   40-60 % and exhibit an *ee* > 90 %. Due to the lack of significant intermolecular interactions, also APA
129   molecules occupy the same adsorption sites as in the case when they are adsorbed without 9-EP (cf. Fig.
130   3).

131   The cycloaddition between APA and 9-EP can be triggered thermally on Pd_1-terminated PdGa{111} by
132   annealing the sample with co-deposited molecules at 425 K. This gives rise to the observation of several
133   new covalently coupled molecular structures (Fig. 4b) in high abundance (Fig. S6-S7). About 5% of the new
134   molecular structures are 9-EP dimers reported in Ref. [37] (blue arrow in Fig. 4b), whereas the remaining 5
135   % consist of one 9-EP molecule and the phenylpropionic acid moiety of APA, but are too small to be intact
136   triazoles (Fig. S8). The vast majority (90 %, green arrows Fig. 4b) of these molecular structures exhibit one
137   of the six different STM appearances presented in Figs. 4c-g. Their STM signature is mainly planar in the
138   vicinity of the coupling site, which excludes them to be 1,5-triazoles, as they would exhibit highly non-
139   planar STM signatures according to DFT calculations done with CP2K[39] within the AiiDalab platform[40] (Fig.
140   S9).

141   To check whether the six molecular structures in Fig. 4c-g are on-surface synthesized 1,4-triazoles, we
142   deposited ex-situ synthesized 1,4-triazoles on A:Pd_1 held at 170 K and 300 K. When imaged with STM, the
143   ex-situ synthesized 1,4-triazoles appear in three inequivalent adsorption configurations (Fig. S10). These
144   1,4-triazole molecules strongly resemble the reaction products formed between APA and 9-EP on the Pd_1-
145   terminated PdGa{111} in terms of shape, dimensions and adsorption geometry (Fig. S11), but differ in the
146   intensity distribution. However, upon annealing the ex-situ synthesized 1,4-triazoles to the reaction
147   temperature of the on-surface synthesis, we observe molecular structures that are identical to those
148   formed between APA and 9-EP on the Pd_1-terminated PdGa{111} surfaces (Fig. S12). This implies that the
149   vast majority of the heterocoupled reaction products are indeed 1,4-triazoles, but with deprotonated
150   carboxylic acid. Hence, the azide-alkyne Huisgen cycloaddition proceeds regioselectively on Pd_1-
151   terminated PdGa{111} surfaces.

152   It becomes clear that the two molecules in Fig. 4c, the two in Figs. 4 d,e and the ones in Figs. 4 f,g are
153   mirror images of each another, thus they represent complementary enantiomers, which will be discussed
154   later in view of enantioselectivity. The distinctive feature in the STM signatures of the R, and S enantiomers
155   in all three cases is the arrangement of the phenylpropionic acid with respect to the phenanthrene moiety.
156   If the phenylpropionic acid unit is perpendicular (almost parallel) to the phenanthrene moiety, the 1,4-
157   triazoles appear L-shaped (Z-shaped) (Fig. 4c-e, the triazoles are denoted P1 and P2, respectively), or I-
158   shaped (P3) for an intermediate orientation (Fig. 4f,g). The atomic resolution of the substrate in the STM
159   images combined with the structure overlay allows to determine the adsorption configuration of these
160   reaction products (Figs. S13 b,e,h), whereas the enantiospecific arrangement of the propionic acid moiety
161   remains ambiguous. The relative abundance of the three product structures P1-P3 are summarized in
162   Table 1 for the two enantiomeric forms R and S on the Pd_1-terminated surfaces (the products are

163 correspondingly labeled R_{P1}, S_{P1}, R_{P2},..., S_{P3}). Regarding the arrangement of the triazole with respect to the
164 phenanthrene moiety in the 1,4-triazoles, P2 and P3 belong to the same diastereomer. Hence the reaction
165 proceeds with a diastereomeric excess $de = 100\% * \frac{P2+P3-P1}{P2+P3+P1}$ of up to 50%. Considering all 1,4-triazoles,
166 the 9-EP moiety appear as racemic mixture, which implies that at the reaction temperature of 425 K, the
167 chiral recognition of 9-EP by the Pd_1-terminated PdGa{111} surfaces has become insignificant. Unlike the
168 Z-shaped products P2, which do not experience any chirality transfer, enantioselectivity is clearly
169 expressed for the L- and I-shaped products P1 and P3, where we find ratios between the different
170 enantiomorphs of up to 4:1 and 5:1, respectively. This enantioselective behavior is supported by deposited
171 ex-situ synthesized 1,4-triazoles pointing towards the same preferential arrangement (cf. Table S6). The
172 opposite ratio between the different P1 and P3 enantiomers for Pd_1-terminated PdGa{111} surfaces of the
173 A and B PdGa crystal enantiomorph strongly corroborates the conclusion of their enantioselective
174 recognition towards the 1,4-triazoles.

175 Compared to investigations of the azide-alkyne Huisgen cycloaddition on Cu(111),[35] where the reaction
176 yield is reported to be of the order of 2-10%, the formation of 1,4-triazoles on the Pd_1-terminated
177 PdGa{111} surfaces reveals a much higher yield of up to 58%. It seems as if this yield depends mainly on
178 the availability of intact APA molecules as the yield increases with increasing ratio between APA/9-EP
179 (Table S7), which is expected in light of the decomposition of the azid group of APA molecules upon
180 deposition on the Pd_1-terminated PdGa{111} surfaces.

181 In summary, we have shown that the azide-alkyne Huisgen cycloaddition between pristine 9-EP and APA
182 occurs regio- and enantioselectively on the Pd_1-terminated PdGa{111} surfaces, i.e., forming exclusively
183 1,4-triazoles with an exceptionally high enantiospecifity of up to 5:1. In view of the d-band model, the Pd_1-
184 terminated PdGa{111} surfaces therefore behave copper-like. On the other hand, the same reaction does
185 not proceed on the Pd_3-terminated PdGa{111} surfaces, even though these PdGa{111} surfaces exhibit
186 very similar electronic d-band structure. We therefore conclude that the vastly dissimilar catalytic
187 properties of the Pd_1- and Pd_3-terminated PdGa{111} surfaces for the azide-alkyne Huisgen cycloaddition
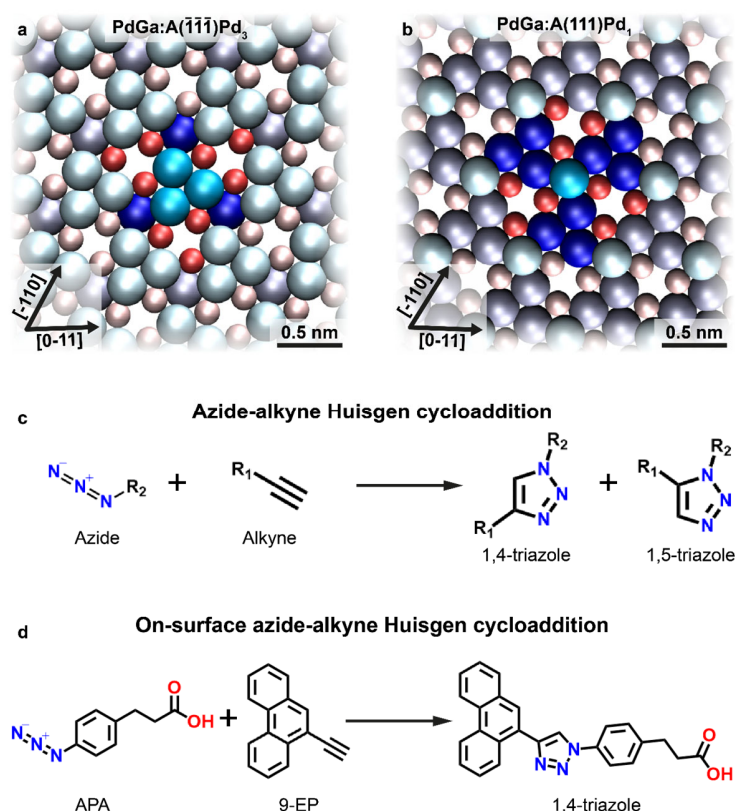188 primarily arise from differences in the atomic arrangement in their terminating layers, i.e., the ensemble
189 effect.

Figure 1 | Schematics of the PdGa{111} surfaces and the azide-alkyne Huisgen cycloaddition

The atomic surface structure of **a** PdGa:A($\overline{1}\overline{1}\overline{1}$)Pd$_3$ (1st layer Pd$_3$ in bright blue: z = 0 pm; 2nd layer Ga$_3$ in red: z = -85 pm; 3rd layer Pd$_1$ in dark blue: z = -161 pm) and **b** PdGa:A(111)Pd$_1$ (1st layer Pd$_1$ in bright blue: z = 0 pm; 2nd layer Ga$_3$ in red: -57.4 pm ; 3rd layer Pd$_3$ in dark blue: -149.8 pm) with their chirality highlighted by a top layer Pd trimer or a single top layer atom, respectively, and their neighbors in saturated colors. **c** General reaction scheme of the azide-alkyne Huisgen cycloaddition. **d** The investigated on-surface Huisgen cycloaddition between 9-ethynylphenanthrene (9-EP) and 3-(4-azidophenyl)propionic acid (APA) yielding 1,4-triazole regioisomers.
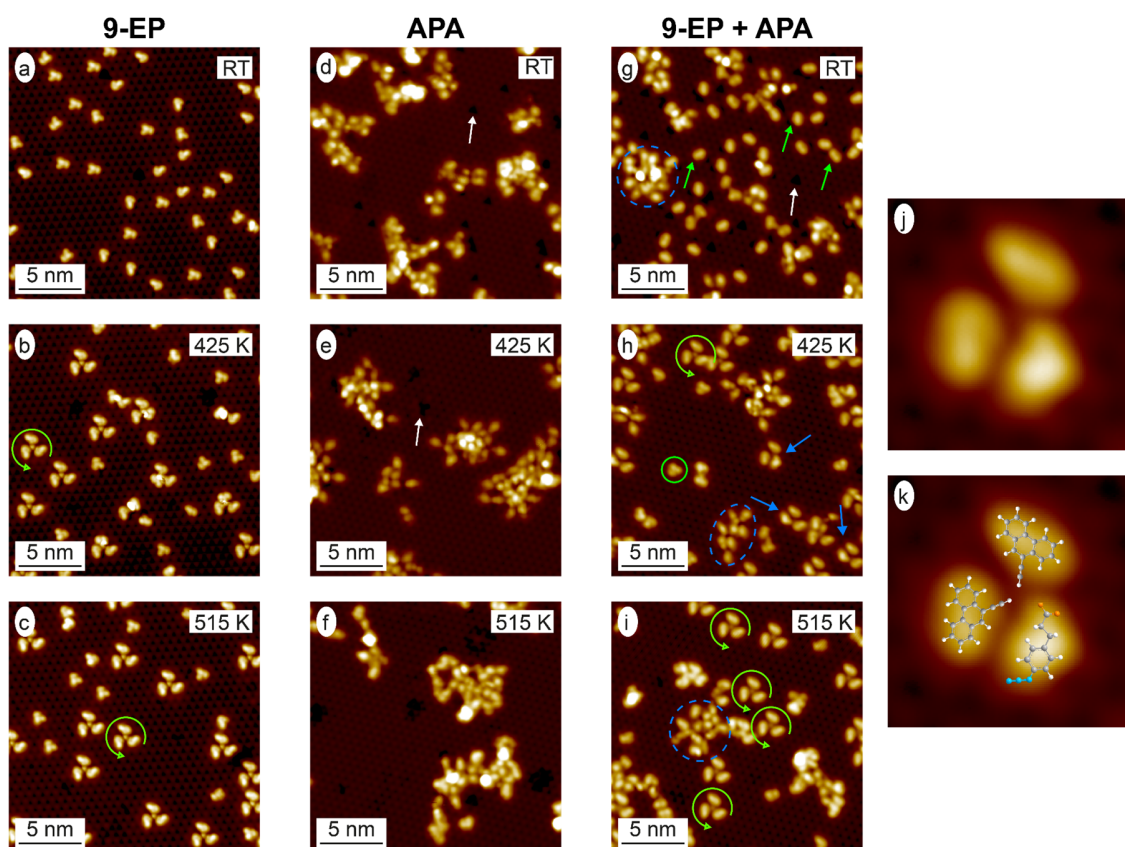
Figure 2 | Suppressed azide-alkyne Huisgen cycloaddition on the Pd$_3$-terminated PdGa{111} surfaces

STM images (V_B = 20 mV; I_T = 1 nA) of 9-EP **a** deposited on PdGa:A($\bar{1}\bar{1}\bar{1}$)Pd$_3$ at RT, and after subsequent annealing to **b** 425 K, and **c** 515 K. STM images (V_B = 200 mV; I_T = 0.1 nA) of APA molecules on the PdGa:A($\bar{1}\bar{1}\bar{1}$)Pd$_3$ surface after **d** RT deposition, subsequent annealing to **e** 425 K, and **f** 515 K. STM images (V_B = 200 mV; I_T = 0.1 nA) of APA co-adsorbed with 9-EP after **g** RT deposition, subsequent annealing to **h** 425 K, and **i** 515 K. High-resolution STM image (3 × 3 nm^2; V_B = 20 mV; I_T = 0.2 nA) of the frequently observed molecular structure containing one APA and two 9-EP molecules, which is marked with blue arrows in **h**, is shown in **j** and overlaid with the molecular structure in **k**. The green circular arrows in **b, c, h, i** highlight the homochiral 9-EP propeller, the white arrows in **d, e, g** the depression caused by APA remnants, and the green arrows in **g** a 9-EP molecule interacting with an APA remnant. The blue dashed circles in **g, h, i** indicate APA agglomerations and the green circle in **h** a 9-EP monomer.
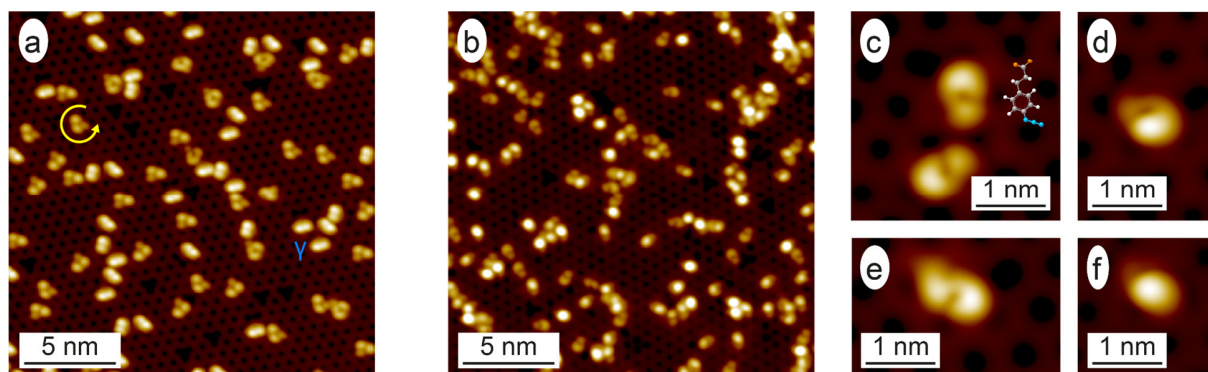
Figure 3 | Alkyne and azide on the Pd$_1$-terminated PdGa{111} surfaces

Large-scale STM images of **a** 9-EP (V$_B$ = 20 mV; I$_T$ = 2 nA) and **b** APA (V$_B$ = 100 mV; I$_T$ = 0.4 nA) deposited at RT on PdGa:A(111)Pd$_1$. **c-f** high resolution STM images (V$_B$ = 20 mV; I$_T$ = 0.2 nA) of the different APA configurations on PdGa:A(111)Pd$_1$ with the molecular structure of APA in **c**.
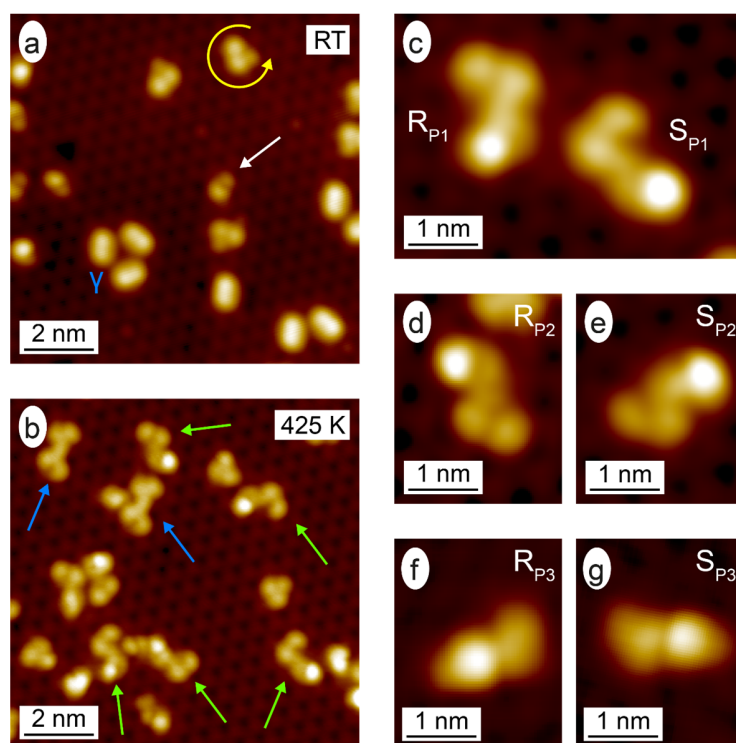
219
220 Figure 4 | Enantioselective azide-alkyne Huisgen cycloaddition on the Pd_1-terminated PdGa{111} surfaces

221 STM images (V_B = -200 mV; I_T = 0.05 nA) of **a** co-deposited APA (white arrow) and 9-EP (yellow arrow and
222 γ-states labelled) molecules on PdGa:B($\overline{1}\overline{1}\overline{1}$)$Pd_1$, and after subsequent annealing to **b** 425 K. In **b**, the 9-EP
223 dimers are pointed out with blue arrows, the 1,4-triazoles with green ones. The different 1,4-triazoles are
224 shown in detail in the high resolution STM images (V_B = -200 mV; I_T = 0.2 nA) in **c-g**. **d** and **g** have been
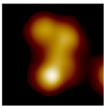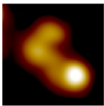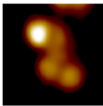225 rotated to highlight the relation of the shown 1,4-triazole to the one in **e** and **f**, respectively.
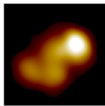226
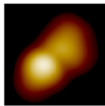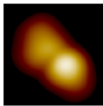
Sample	1,4-triazoles						9-EP dimer	Others
	R_{P1}	S_{P1}	R_{P2}	S_{P2}	R_{P3}	S_{P3}		
A:Pd$_1$	5 ± 1%	21 ± 2%	13 ± 2%	14 ± 2%	30 ± 2%	6 ± 1%	6 ± 1%	5 ± 1%
B:Pd$_1$	18 ± 2%	3 ± 1%	10 ± 2%	10 ± 2%	12 ± 2%	36 ± 2%	5 ± 1%	6 ± 1%

Table 1 | Quantification of the reaction products

Abundancies of the identified coupled molecular species on the PdGa:A(111)Pd$_1$ and PdGa:B($\bar{1}\bar{1}\bar{1}$)Pd$_1$ surfaces. The reaction products P1 and P3 clearly occur enantioselectively, while the products P2 appear in a racemic mixture.

233   References

234   1.   Clair, S. & de Oteyza, D. G. Controlling a Chemical Coupling Reaction on a Surface: Tools and Strategies

235   for On-Surface Synthesis. *Chem. Rev.* **119**, 4717–4776 (2019).

236   2.   Smith, S. W. Chiral Toxicology: It's the Same Thing... Only Different. *Toxicol. Sci.* **110**, 4–30 (2009).

237   3.   Kasprzyk-Hordern, B. Pharmacologically active compounds in the environment and their chirality.

238   *Chem. Soc. Rev.* **39**, 4466–4503 (2010).

239   4.   Stacchiola, D., Burkholder, L. & Tysoe, W. T. Enantioselective Chemisorption on a Chirally Modified

240   Surface in Ultrahigh Vacuum: Adsorption of Propylene Oxide on 2-Butoxide-Covered Palladium(111).

241   *J Am Chem Soc* **124**, 8984–8989 (2002).

242   5.   Lee, I. & Zaera, F. Chiral Templating of Surfaces: Adsorption of (S)-2-Methylbutanoic Acid on Pt(111)

243   Single-Crystal Surfaces. *J Am Chem Soc* **128**, 8890–8898 (2006).

244   6.   Gao, F., Wang, Y., Li, Z., Furlong, O. & Tysoe, W. T. Enantioselective Reactions on a Au/Pd(111) Surface

245   Alloy with Coadsorbed Chiral 2-Butanol and Propylene Oxide. *J Phys Chem C* **112**, 3362–3372 (2008).

246   7.   Demers-Carpentier, V. *et al.* Direct Observation of Molecular Preorganization for Chirality Transfer on

247   a Catalyst Surface. *Science* **334**, 776–780 (2011).

248   8.   Lawton, T. J. *et al.* Long Range Chiral Imprinting of Cu(110) by Tartaric Acid. *J Phys Chem C* **117**, 22290–

249   22297 (2013).

250   9.   Dutta, S. & Gellman, A. J. Enantiomer surface chemistry: conglomerate versus racemate formation on

251   surfaces. *Chem. Soc. Rev.* **46**, 7787–7839 (2017).

252   10. Zaera, F. Chirality in adsorption on solid surfaces. *Chem. Soc. Rev.* **46**, 7374–7398 (2017).

253   11. Meemken, F. & Baiker, A. Recent Progress in Heterogeneous Asymmetric Hydrogenation of C═O and

254   C═C Bonds on Supported Noble Metal Catalysts. *Chem. Rev.* **117**, 11522–11569 (2017).

255   12. McFadden, C. F., Cremer, P. F. & Gellman, A. J. Adsorption of Chiral Alcohols on 'Chiral' Metal Surfaces.

256   *Langmuir* **12**, 2483–2487 (1996).

257   13. Sholl, D. S. & Gellman, A. J. Developing Chiral Surfaces for Enantioselective Chemical Processing. *AIChE*

258   *J.* **55**, 2484–2490 (2009).

259   14. Gellman, A. J. *et al.* Superenantioselective Chiral Surface Explosions. *J Am Chem Soc* **135**, 19208–19214

260   (2013).

261   15. Mhatre, B. S., Dutta, S., Reinicker, A., Karagoz, B. & Gellman, A. J. Explosive enantiospecific

262   decomposition of aspartic acid on Cu surfaces. *Chem Commun* **52**, 14125–14128 (2016).

263   16. Sanchez, D. S. *et al.* Topological chiral crystals with helicoid-arc quantum states. *Nature* **567**, 500–505

264   (2019).

265   17. Rao, Z. *et al.* Observation of unconventional chiral fermions with long Fermi arcs in CoSi. *Nature* **567**,

266   496–499 (2019).

267   18. Lv, B. Q. *et al.* Observation of multiple types of topological fermions in PdBiSe. *Phys. Rev. B* **99**, 241104

268   (2019).

269   19. Schröter, N. B. M. *et al.* Chiral topological semimetal with multifold band crossings and long Fermi

270   arcs. *Nat. Phys.* **15**, 759–765 (2019).

271   20. Yuan, Q.-Q. *et al.* Quasiparticle interference evidence of the topological Fermi arc states in chiral

272   fermionic semimetal CoSi. *Sci. Adv.* **5**, eaaw9485 (2019).

273   21. Schröter, N. B. M. *et al.* Observation and control of maximal Chern numbers in a chiral topological

274   semimetal. *Science* **369**, 179–183 (2020).

275   22. Yao, M. *et al.* Observation of giant spin-split Fermi-arc with maximal Chern number in the chiral

276   topological semimetal PtGa. *Nat. Commun.* **11**, 2033 (2020).

277   23. Sessi, P. *et al.* Handedness-dependent quasiparticle interference in the two enantiomers of the

278   topological chiral semimetal PdGa. *Nat. Commun.* **11**, 3507 (2020).

279   24. Armbrüster, M. *et al.* Refinement of the crystal structure of palladium gallium (1:1), PdGa. *Z Krist. NCS*

280   **225**, 617–618 (2010).

281   25. Rosenthal, D. *et al.* Surface Investigation of Intermetallic PdGa(-1-1-1). *Langmuir* **28**, 6848–6856

282   (2012).

283   26. Prinz, J. *et al.* Isolated Pd sites on the intermetallic PdGa(111) and PdGa(-1-1-1) model catalyst

284   surfaces. *Angew. Chem.* **124**, 9473–9477 (2012).

285   27. Sachtler, W. M. H. Chemisorption Complexes on Alloy Surfaces. *Catal. Rev. - Sci. Eng.* **14**, 193–210

286   (1976).

287   28. Liu, P. & Nørskov. Ligand and ensemble effects in adsorption on alloy surfaces. *Phys Chem Chem Phys*

288   **3**, 3814–3818 (2001).

289   29. Prinz, J. *et al.* Ensemble Effect Evidenced by CO Adsorption on the 3-Fold PdGa Surfaces. *J. Phys. Chem.*

290   *C* **118**, 12260–12265 (2014).

291   30. Prinz, J. *et al.* Adsorption of Small Hydrocarbons on the Three-Fold PdGa Surfaces: The Road to

292   Selective Hydrogenation. *J. Am. Chem. Soc.* **136**, 11792–11798 (2014).

293   31. Stolz, S., Gröning, O., Prinz, J., Brune, H. & Widmer, R. Molecular motor crossing the frontier of classical

294   to quantum tunneling motion. *Proc. Natl. Acad. Sci.* **117**, 14838–14842 (2020).

295   32. Prinz, J. Surface Science Investigations on Structure and Binding Centers of Intermetallic PdGa

296   Surfaces. (EPFL, 2014).

297   33. Stolz, S. *et al.* Near-enantiopure trimerization of 9-Ethynylphenanthrene on a chiral metal surfce.

298   *Angew. Chem. Int. Ed.* **59**, 18179–18183 (2020).

299   34. Diaz Arado, O. *et al.* On-Surface Reductive Coupling of Aldehydes on Au(111). *Chem. Commun.* (2015)

300   doi:10.1039/C4CC09634G.

301   35. Bebensee, F. *et al.* On-Surface Azide–Alkyne Cycloaddition on Cu(111): Does It "Click" in Ultrahigh

302   Vacuum? *J. Am. Chem. Soc.* **135**, 2136–2139 (2013).

303   36. Nørskov, J. K. *et al.* The nature of the active site in heterogeneous metal catalysis. *Chem Soc Rev* **37**,

304   2163–2171 (2008).

305   37. Prinz, J., Gröning, O., Brune, H. & Widmer, R. Highly Enantioselective Adsorption of Small Prochiral

306   Molecules on a Chiral Intermetallic Compound. *Angew. Chem. Int. Ed.* **54**, 3902–3906 (2015).

307   38. Hellerstedt, J. *et al.* Aromatic Azide Transformation on the Ag(111) Surface Studied by Scanning Probe

308   Microscopy. *Angew Chem Int Ed* **58**, 2266–2271 (2019).

309   39. Hutter, J., Iannuzzi, M., Schiffmann, F. & Vandevondele, J. Cp2k: Atomistic simulations of condensed

310   matter systems. *Wiley Interdiscip. Rev. Comput. Mol. Sci.* **4**, 15–25 (2014).

311   40. Pizzi, G., Cepellotti, A., Sabatini, R., Marzari, N. & Kozinsky, B. AiiDA: automated interactive

312   infrastructure and database for computational science. *Comput. Mater. Sci.* **111**, 218–230 (2016).

313

314

ASSOCIATED CONTENT

Supporting Information

The Supporting Information containing additional experimental results is available free of charge on the Wiley Publications website.

AUTHOR INFORMATION

Author contributions

RW conceived and initiated the project in collaboration with HB and OG. SS performed the measurements with assistance of NK, MaB, ET, NB, AK, NMD, RW, and performed the DFT calculations under the supervision of CAP and analyzed the data under supervision of RW. MiB synthesized the ex-situ 1,4-triazoles under the supervision of RH. SS wrote the manuscript with input from all co-authors.

Corresponding Authors
*E-mail: roland.widmer@empa.ch

ORCID
Roland Widmer: 0000-0002-9226-3136
Samuel Stolz: 0000-0002-3597-680X
Harald Brune: 0000-0003-4459-3111

Notes
The authors declare no competing financial interest

ACKNOWLEDGMENTS